RESEARCH ARTICLE

Quantitative and Visual Assessments toward Potential Sub-mSv or Ultrafast FDG PET Using High-Sensitivity TOF PET in PET/MRI

Spencer C. Behr,[1] Emma Bahroos,[1] Randall A. Hawkins,[1] Lorenzo Nardo,[2] Vahid Ravanfar,[1] Emily V. Capbarat,[1] Youngho Seo[1,3]

[1]Department of Radiology and Biomedical Imaging, UCSF, 185 Berry Street, Suite 350, San Francisco, CA, 94107, USA
[2]Department of Radiology and Biomedical Engineering, Davis Medical Center, University of California, San Francisco, CA, USA
[3]Department of Radiation Oncology, University of California, San Francisco, CA, USA

Abstract

Purpose: Newer high-performance time-of-flight (TOF) positron emission tomography (PET) systems have the capability to preserve diagnostic image quality with low count density, while maintaining a high raw photon detection sensitivity that would allow for a reduction in injected dose or rapid data acquisition. To assess this, we performed quantitative and visual assessments of the PET images acquired using a highly sensitive (23.3 cps/kBq) large field of view (25-cm axial) silicon photomultiplier (SiPM)-based TOF PET (400-ps timing resolution) integrated with 3 T-MRI in comparison to PET images acquired on non-TOF PET/x-ray computed tomography (CT) systems.
Procedures: Whole-body 2-deoxy-2-[^{18}F]fluoro-D-glucose ([^{18}F]FDG) PET/CT was acquired for 15 patients followed by whole body PET/magnetic resonance imaging (MRI) with an average injected dose of 325 ± 84 MBq. The PET list mode data from PET/MRI were reconstructed using full datasets (4 min/bed) and reduced datasets (2, 1, 0.5, and 0.25 min/bed). Qualitative assessment between PET/CT and PET/MR images were made. A Likert-type scale between 1 and 5, 1 for non-diagnostic, 3 equivalent to PET/CT, and 5 superior quality, was used. Maximum and mean standardized uptake values (SUV$_{max}$ and SUV$_{mean}$) of normal tissues and lesions detected were measured and compared.
Results: Mean visual assessment scores were 3.54 ± 0.32, 3.62 ± 0.38, and 3.69 ± 0.35 for the brain and 3.05 ± 0.49, 3.71 ± 0.45, and 4.14 ± 0.44 for the whole-body maximum intensity projections (MIPs) for 1, 2, and 4 min/bed PET/MR images, respectively. The SUV$_{mean}$ values for normal tissues were lower and statistically significant for images acquired at 4, 2, 1, 0.5, and 0.25 min/bed on the PET/MR, with values of − 18 ± 28 % ($p < 0.001$), − 16 ± 29 % ($p = 0.001$), − 16 ± 31 % ($p = 0.002$), − 14 ± 35 % ($p < 0.001$), and − 13 ± 34 % ($p = 0.002$), respectively. SUV$_{max}$ and SUV$_{peak}$ values of all lesions were higher and statistically significant ($p < 0.05$) for 4, 2, 1, 0.50, and 0.25 min/bed PET/MR datasets.
Conclusion: High-sensitivity TOF PET showed comparable but still better visual image quality even at a much reduced activity in comparison to lower-sensitivity non-TOF PET. Our data translates to a seven times reduction in either injection dose for the same time or total scan time for the same injected dose. This "ultra-sensitivity" PET system provides a path to clinically acceptable extremely low-dose FDG PET studies (e.g., sub 1 mCi injection or sub-mSv effective dose) or PET studies as short as 1 min/bed (e.g., 6 min of total scan time) to cover whole body without compromising diagnostic performance.

Key words: PET, PET/MRI, PET/CT, TOF, Sub-mSv, High-sensitivity, Timing resolution, Ultrafast

Correspondence to: Emma Bahroos; *e-mail:* Emma.Bahroos@ucsf.edu

Introduction

Over the years, there have been steady technological advancements made to the positron emission tomography (PET) detectors to improve the imaging performance. Improvements in hardware such as fast photodetectors, along with fast scintillation crystals such as lutetium-based scintillators (e.g., lutetium orthosilicate and lutetium-yttrium oxyorthosilicate) and fast computing for image reconstruction algorithms have improved the time-of-flight (TOF) performance and its adoption in clinical PET imaging [1, 2].

In conventional PET imaging, lines of response (LOR) are obtained at multiple angles to construct a tomographic image through an iterative process. With TOF PET, in addition to determining the LOR for each annihilation event, it measures the time each coincidence photon was detected and calculates the arrival time difference. This difference helps determine the position of annihilation along the LOR and thus help improve the image signal-to-noise ratio (SNR) [1].

Most of the current clinical TOF PET detectors have a timing resolution of about 500–600 ps [1]. There has been a gradual improvement in the TOF performance, from a timing resolution of 585 ps to less than 400 ps [1, 3]. Another recent clinical TOF PET (Vereos, Philips Healthcare) using one-to-one matching crystal to silicon photomultiplier (SiPM) readout reports 316 ps on average timing resolution of TOF [4], which is considered the current state-of-the-art among commercially available PET/ x-ray computed tomography (CT) systems. In research settings, there has been active development of prototype systems that further push the limits of timing resolution and the ability to accurately quantify the number of counts and allowing for ultrafast acquisition times [5–7].

The sensitivity gain from improved TOF performance is related to the object size, so that the greatest gain is found in heavier patients. With non-TOF PET detectors, imaging heavier patients has been difficult, as attenuation renders poor quality images resulting in lower lesion detectability. Recent studies have shown TOF PET improves overall image quality and results in a significant SNR gain in patient studies [8–10]. Improved SNR has demonstrated better lesion detection, especially in a higher background setting [11–13]. TOF images acquired at 40 % lower scan time than the conventional non-TOF images were comparable in lesion detection [13–15]. In a study examining the impact of TOF in [18F]fluorocholine PET/ CT prostate cancer patients by Hausmann et al., additional lesions were detected using TOF PET and the demarcation quality of the lesions was also improved [16]. However, most of these TOF vs. non-TOF comparison studies were based on TOF PET systems with 500–600 ps timing resolution.

More recently, the PET subsystem of an integrated PET/ magnetic resonance imaging (MRI) system (SIGNA PET/MR, GE Healthcare) using SiPM as its PET photodetector showed TOF performance with a timing resolution of less than 400 ps. In addition, this PET/MRI system maintains a thick crystal (25 mm) with a large axial coverage (25 cm) so that its raw photon detection sensitivity at the center of field of view (FOV) is reported at 23.3 cps/kBq [17]. The combination of high sensitivity and good TOF timing resolution should be able to capture reasonably reconstructed clinical images with much less activity than normally performed using a non-TOF PET scanner that also does not have the high sensitivity. The utilization of 500 ps TOF PET has already allowed administered activity to be at least 30 % lower [14] than when imaging with a non-TOF PET detector. The effective dose received by a patient during a 2-deoxy-2-[18F]fluoro-D-glucose ([18F]FDG) PET scan is 0.7 mSv/mCi [18] and with current ongoing advancements in TOF technology, we can expect a significant reduction in the injected activity along with faster imaging.

The purpose of this study is to compare the PET images obtained from non-TOF PET/CT scanners with the PET images obtained from TOF PET/MR using metrics like standardized uptake values (SUVs), visual image quality assessment, and lesion detection capability. We believe that the highly sensitive, large axial field of view (25 cm) SiPM-based TOF-PET (400 ps timing resolution) offers the possibility of extremely low-dose or extremely rapid diagnostic-quality images.

Materials and Method

The study was approved by the local institutional review board (IRB), and a written informed consent was obtained from all patients before the examinations. Fifteen patients scheduled for a clinically indicated [18F]FDG PET/CT were recruited as part of this study. PET/MR studies were performed immediately following the whole-body [18F]FDG PET/CT. There was no second administration of [18F]FDG for PET/MRI studies.

All PET scans were acquired using the standard clinical protocol at our institution. Patients were injected with the standard activity of [18F]FDG (5.2 MBq/kg). Prior to radiotracer injection, all patients fasted for at least 6 h, and blood glucose was checked to confirm levels less than 200 mg/dl. A total of 15 patients were selected (7 females). The average age of the participants was 61 ± 12 years (ranging from 29 to 81 years) and had a mean weight of 78.75 ± 20.18 kg (ranging from 50 to 120 kg). All PET/CTs were referred for oncologic indications including; melanoma (10 subjects), diffuse large B cell lymphoma (2 subjects), ovarian cancer (rising tumor markers), metastatic gastrointestinal stromal tumor, and metastatic cholangiocarcinoma. The average [18F]FDG dose injected was 325 ± 84 MBq. We used the effective dose of 0.019 mSv/MBq relationship to calculate the radiation exposure to each subject due to the injected [18F]FDG [19]. PET/CT images were acquired after a mean uptake time of 65 ± 10 min. PET/MR images were acquired 152 ± 27-min post [18F]FDG injection. Three patients did not fully complete the PET/MR examination. Head and neck imaging was performed on all 15 patients. Two patients did not complete chest, abdomen, and pelvis, and one did not complete abdomen and chest but did complete head, neck, and pelvis.

PET/CT Technique

PET/CT examinations were either performed on Discovery VCT PET/CT (GE Healthcare) or Biograph HiRez 16 (Siemens Healthcare). The PET/CT scanners utilized for this study do not have TOF capability and were previously calibrated with standardized phantoms. Our standard PET acquisition is eight bed stations to cover the vertex of the skull to mid-thigh and 3–4 min per bed station. PET reconstructions were performed using the vendor-provided iterative reconstruction algorithm using CT-based AC with a matrix of 168 × 168 and a slice thickness of 5.00 mm for images acquired on the Biograph HiRez 16 and a matrix of 128 × 128 with a slice thickness of 3.27 mm for images acquired on the Discovery VCT PET/CT. Helical CT scans were performed for PET attenuation correction (AC) and reconstructed with a transverse FOV of 500 or 700 mm, a slice thickness of 3.75 (Discovery VCT) or 5.00 mm (Biograph HiRez 16), and a matrix size of 512 × 512. Eleven subjects were imaged on the Discovery VCT and four on the Biograh HiRez 16.

PET/MR Technique

Patients were all screened for MRI compatibility per department MRI safety protocol for any contraindications or claustrophobia prior to being enrolled. Immediately upon completion of the PET/CT, the TOF-PET/MR acquisition was performed on SIGNA PET/MR (GE Healthcare). The PET system has a cylindrical geometry and consists of LYSO scintillator crystals paired with SiPMs. The timing resolution of this scanner as per the manufacturer is less than 400 ps. The details of this scanner have been reported in previous studies [17]. A total of six bed stations were acquired per patient to cover the vertex of the skull to the mid thighs. Each PET bed station took 4 min, with a transverse matrix of 192 × 192 and a slice thickness of 2.78 mm. While PET data were acquired, a 3D dual-echo, spoiled gradient echo sequence with two-echo-based Dixon fat-water separation was acquired using combination of a head and neck coil and two body coils. The atlas-based AC including the pre-determined head coil in the attenuation map was applied to PET reconstruction for the head region, and the Dixon images, but not including the body coils, were used to calculate the attenuation map for AC in PET reconstruction of the body other than the head. This sequence generated volumetric images of in-phase, out-phase, fat, and water with a transaxial FOV of 500 mm, a slice thickness of 5.2 mm, a slice spacing of 2.6 mm, and a matrix size of 256 × 256 × 120 per each bed station. Because of the smaller transverse FOV from the Dixon MRI, the truncation resulted from Dixon-based attenuation map was compensated from the boundaries defined by PET reconstruction without AC. The MRI images for MR-based attenuation correction (MRAC) were acquired simultaneously with PET, and were less than 20 s per bed position.

PET reconstruction was performed using TOF and MRAC acquired from the two-echo Dixon fat-water separation. In order to simulate the low-dose/fast-acquisition schemes, five additional unique PET datasets were reconstructed by including only a portion of the acquired data from the listmode data: 4 (100 % of the data), 2 (50 %), 1 (25 %), 0.5 (12.5 %), and 0.25 (6.25 %) min per bed station. PET images were performed with TOF-OSEM with two iterations and 28 subsets. The dataset of one subject included 3, 2, 1, 0.5, and 0.25 min/bed reconstructions and these 3-min images were grouped with the 4 min/bed image dataset.

Image Review

Qualitative Assessment   Full-body maximum intensity projection (MIP) images and a single axial PET image through the level of the thalamus was created. Each patient's PET/CT MIP and axial PET image was then compared to various PET/MR time point (100 % of the data to 6.25 %) reconstruction. The PET/CT was considered the reference standard to be classified as diagnostic. A dual board-certified (in diagnostic radiology and nuclear medicine) physician with over 30 years of reading PET, a dual board-certified junior attendee with 10 years of experience, and a nuclear medicine resident with 5 years of experience compared the PET/CT to the various PET/MR images obtained from the full datasets and the subsets of them. Each PET/MR was compared to the PET/CT from the same patient. The readers knew the identity of the scan from the PET/CT and PET/MR, but were blinded to the amount of the datasets used (full or subset). They scored each set of times on a Likert-type scale 1 to 5: 1 = non-diagnostic, 2 = quality less than PET/CT, 3 = equal to PET/CT, 4 = quality better than PET/CT, and 5 = significantly better quality than PET/CT and/or new lesions seen. To avoid potential recall, the images were randomized and only PET images of both modalities were reviewed.

PET Analysis   A fellowship-trained radiologist in nuclear medicine with over 10 years of reading PET reviewed each PET study on an OsiriX v8.0. MIP, axial, sagittal, and coronal PET images and fused images were reviewed. For the PET/CT, PET images were fused with the diagnostic CT images performed during the same examination. For the PET/MR studies, PET images were fused with both the T1- and T2-weighted axial MRI images obtained during the PET/MR examination. A 1-centimeter volume of interest was drawn over normal tissue that included the right cerebellar hemisphere, right parotid gland, humeral head, lung, ascending aorta, gluteal fat, and gluteal muscles for the PET from the PET/CT as well as each time point from the PET/MR reconstructions. The SUV_{max} and SUV_{mean} values were recorded. For each PET study, the location, SUV_{max} and SUV_{peak} of each PET avid lesion were recorded for each patient. PET-positive lesions were considered positive if it was clearly seen above adjacent soft tissue and had a clear cross sectioning correlate.

Statistical Analysis The SUV mean and maximum values of PET/MR images at each duration, 4, 2, 1, 0.50, and 0.25 min were compared to the SUV's of the PET/CT images acquired at 4 min using a two-tailed paired t test. Difference in SUV_{mean}, SUV_{max}, and SUV_{peak} were compared between PET/CT and each PET/MR dataset and treated as separate outcomes. Bonferroni's correction was utilized for multiple comparisons. A p value smaller than 0.05 was considered statistically significant when evaluating normal tissue and the detected lesions on the two different PET scanners.

Results

Based on effective dose of 0.019 mSv/MBq estimation for FDG, the mean radiation exposure for our subjects, excluding the additional dose from CT, was 6.2 ± 1.6 mSv, ranging from 3.7 to 8.9 mSv.

Qualitative Results

Results of the quality assessment are summarized in Table 1. Overall, PET/MR image quality was considered equal to that of the compared PET/CT even at 1 min/bed data (equivalent total PET acquisition time = 6 min) for the whole-body MIP images with a mean score of 3.05 ± 0.49. For the 2 min/bed (equivalent total PET acquisition time + 12 min) reconstructions, the axial image through thalamus resulted in a mean score of 3.62 ± 0.38 in the quality assessment. The visual assessment comparison is compiled in Figs. 1 and 2.

SUV Analysis

Normal Tissue The SUV_{max} values for all the normal tissue examined are lower for the 4- and 2-min PET/MR images, -13 ± 35 % ($p = 0.044$) and -6 ± 35 % ($p = 6.168$) and higher for the 1, 0.5, and 0.25 min/bed images, 11 ± 43 % ($p = 0.080$), 40 ± 79 % ($p < 0.001$), 74 ± 95 % ($p < 0.001$), respectively, when compared to the SUV_{max} from the standard PET/CT images. The difference between these values was statistically significant except for the SUV_{max} values of the 4, 2, and 1 min/bed PET/MR images. For image acquisitions, less than 1 min/bed had increasing noise that resulted in increased SUV_{max} variability. SUV_{mean} values, on the other hand, for normal tissues were lower and statistically significant for images acquired at 4, 2, 1, 0.5, and 0.25 min/bed on the PET/MR(TOF), with values of -18 ± 28 % ($p < 0.001$), -16 ± 29 % ($p = 0.001$), -16 ± 31 %($p = 0.002$), -14 ± 35 % ($p < 0.001$), and -13 ± 34 % ($p = 0.002$), respectively.

The overall PET/MR SUV_{max} values for normal tissues were lower, with the exception of brain and parotid, where there was no significant difference from the PET/CT. As mentioned before, the SUV_{mean} values were significantly lower on all PET/MR and significantly different for humerus, aorta, lung, spleen, and liver than the PET/CT.

Lesions Abnormal uptake on either PET/CT or PET/MR was seen on 8 patients out of 15. A total of 41 lesions were detected. One cutaneous lesion in the head and neck region was not seen on the PET/CT but seen on the PET/MR at 4, 2, and 1 min/bed reconstructed images. The number of lesions detected are summarized in (Table 2).

For each lesion, the volume, the SUV_{peak}, and SUV_{mean} values were measured. Five of these lesions had either total metabolic volumes less than 1 cm or uptake similar to background on the PET/CT for SUV_{peak} and SUV_{mean} measurements. For these lesions, the SUV_{peak} was higher on the PET/MR images. The SUV_{max} values of all lesions detected on the PET/MR TOF were higher and statistically significant ($p < 0.001$) for 4, 2, 1, 0.50, and 0.25 min/bed images, 56 ± 66, 65 ± 69, 77 ± 69, 101 ± 81, and 116 ± 86 %, respectively, compared to PET/CT. The SUV_{peak} values for all lesions seen the images acquired on the PET/MR TOF 4, 2, 1, 0.50, and 0.25 min images were 39 ± 43 % ($p < 0.001$), 43 ± 48 % ($p < 0.001$), 48 ± 49 % ($p < 0.001$), 48 ± 52 % ($p = 0.003$), and 40 ± 48 % ($p = 0.007$), respectively.

Discussion

In this study, we evaluated the performance of the TOF PET/MR in comparison to non-TOF PET/CT PET detectors, and the large axial field of view of TOF PET/MR. We assessed the image quality and conducted region of interest (ROI)-based analysis of normal tissues and detected lesions. The images acquired with the TOF PET/MRI are greater in overall image quality when compared to that of PET/CT. PET/MR images acquired at the at the same duration as the PET/CT (total of 24 min of PET acquisition: 4 min/bed for six beds for PET/

Table 1. Results of the quality assessment

		0.25 min	0.50 min	1 min	2 min	4 min
Whole-body MIP	SA	2.08 ± 0.38	2.38 ± 0.52	2.92 ± 0.41	3.64 ± 0.50	4.17 ± 0.43
	JA	2.15 ± 0.28	2.54 ± 0.51	3.00 ± 0.86	3.64 ± 0.63	4.00 ± 0.72
	NM	2.23 ± 0.44	2.38 ± 0.51	2.32 ± 0.73	3.86 ± 0.66	4.25 ± 0.75
Brain	SA	2.54 ± 0.38	3.00 ± 0.48	3.38 ± 0.38	3.38 ± 0.55	3.69 ± 0.60
	JA	2.15 ± 0.66	2.69 ± 0.71	3.15 ± 0.77	3.85 ± 0.51	3.77 ± 0.48
	NM	3.46 ± 0.88	3.85 ± 0.69	4.08 ± 0.49	3.62 ± 0.51	3.62 ± 0.65

SA senior attending, *JA* junior attending, *NM* nuclear medicine resident. Score: *1* non-diagnostic, *2* quality less than PET/CT, *3* equal, *4* quality better than PET/CT, *5* significantly better quality than PET/CT and/or new lesions seen
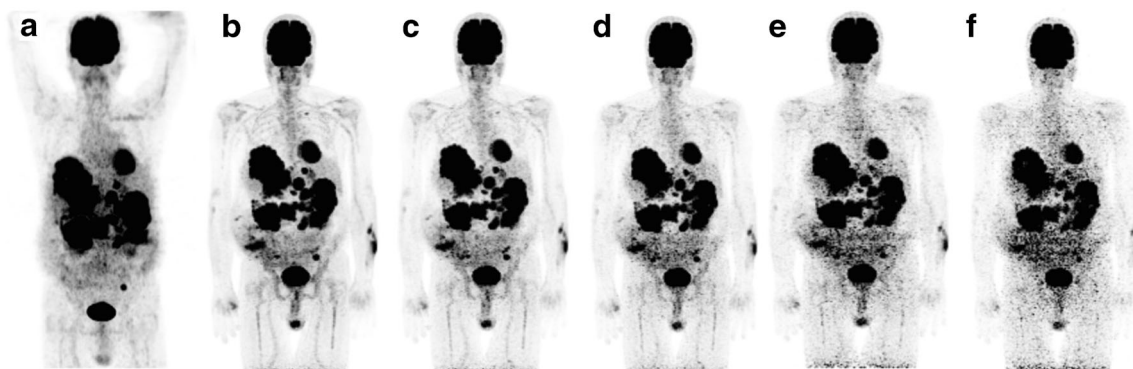
Fig. 1 Whole-body MIPs acquired on the PET/CT and as well as on the PET/MR. image acquisition done on the PET/MR was at 4, 2, 1, 0.50, and 0.25 min per bed position. Images show a comparison between standard non-TOF PET/CT images and the TOF PET/MR. **a** PET/CT. **b** 4-min PET/MR. **c** 2-min PET/MR. **d** 1-min PET/MR. **e** 0.50-min PET/MR. **f** 0.25 min PET/MR.

MRI and 3 min/bed for eight beds for PET/CT), showed better image quality, despite being acquired about 2.5 h after the [18F]FDG injection. Image quality scores summarized in Table 1 show reduced acquisition time to 1 min/bed on the PET/MR still provided comparable quality, indicating that comparable PET image quality can be acquired in either much shorter time or lower dose. MIPs were utilized to overall image quality as well as low count areas instead of the axials, which are good for the assessment of anatomical details.

Increased [18F]FDG uptake relative to normal tissue is a useful marker for many types of cancers. SUV is an index that takes into account the variations in the injected dose and patient's weight to determine the relative measure of [18F]FDG uptake and is commonly used for comparing scans [20]. It is important to note that SUVs are a semi-quantitative measure of FDG uptake and a suggested tool for diagnosis. The overall SUV values of the normal tissues on PET/MR were lower than the PET/CT values, as expected because of the further clearance of FDG in these tissues at a later time point. In addition, reconstruction is better at low background than high, which also plays a role in improved PET/MR image quality. The SUV_{mean} for all normal tissues is summarized in Fig. 3.

The aorta, liver, and spleen have shown to have decreased activity concentration from 1 to 2 h and parotid glad has shown to have no significant change over time [21], which is consistent with our findings. Furthermore, PET/MR uses different AC methods for head and body. Atlas-based AC method is used for the head and four-segment tissue classification for the body, and this difference may have also

contributed to the slight differences in the standard uptake values.

Despite PET/MR images being acquired about 2.5 h post administration of the tracer, all lesions that were detected on the PET/CT were also seen on the PET/MR. This is expected with an extended uptake time [22], but also attributed to the higher sensitivity provided by the TOF PET [23, 24]. This study only detected one additional lesion on the PET/MR, other studies have shown increased detectability with TOF PET detectors or later (delayed) imaging time points. One of the studies compared non-TOF PET to 500-ps TOF PET detectors [16] and another was a pilot study comparing non-TOF PET to 400 ps TOF PET [25]. Though the focus of this study was to assess the overall image quality of images from TOF vs. non-TOF PET detector, we did see that small lesions, similar to background, were better seen on all acquisition times on the PET/MR. Our SUV_{max} and SUV_{peak} for small lesion with mean tumor volume of less than 3 cm, were statistically significant (except for PET/MR at 25 s bed position SUV_{peak}) and supported finding by Koopman et al. [26]. However, since the differences in the reported spatial resolution measurements between these PET/CTs and the PET/MR are small, we also consider that the different time points of imaging (early vs. delayed scan) should have contributed greatly in the SUV differences [22]. The SUV_{max} and SUV_{peak} values of all the detected lesions is summarized in Figs. 4 and 5, respectively.

Though the SUV_{max} depicts the maximum metabolic activity, it is considered a single-pixel ROI and therefore is subject to greater variations and lacks good reproducibility.
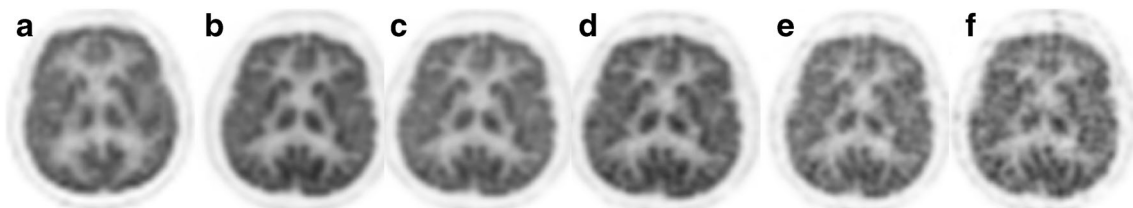
Fig. 2 Brain images acquired on the PET/CT and on the PET/MR. Image acquisition done on the PET/MR was at 4, 2, 1, 0.50, and 0.25 min per bed position. Images show a comparison between standard non-TOF PET/CT images and the TOF PET/MR. **a** PET/CT. **b** 4-min PET/MR. **c** 2-min PET/MR. **d** 1-min PET/MR; **e** 0.50-min PET/MR. **f** 0.25-min PET/MR.

Table 2. Summary of the number of lesions detected in PET/CT (non-TOF) and PET/MR (TOF) 3+, 2, 1, 0.50, 0.25 min images

	PET/CT	4 min	2 min	1 min	0.50 min	0.25 min
Lesion location						
Abdomen/pelvis	17	17	17	17	17	14
Head and neck	14	15	15	15	13	11
Chest	9	9	9	7	7	5
Total	40	41	41	39	37	30
Lesion type/location						
Brown fat	5	5	5	5	5	5
Cutaneous	1	2	2	2	1	1
Lymph node	9	9	9	9	8	6
Oropharynx	2	2	2	2	2	1
Ovary	1	1	1	1	1	1
Adrenal	1	1	1	1	1	1
Parotid	3	3	3	3	3	2
Peritoneal implant	9	9	9	9	9	9
Pulmonary nodule	4	4	4	2	2	2
Rib fracture	2	2	2	2	2	0
Subcutaneous	3	3	3	3	3	2
Total	40	41	41	39	37	30

Fluctuations in the SUV_{max} values are accentuated with the increase in matrix size and a reduction in counts [27]. The statistical reproducibility of the SUV_{mean} and SUV_{peak} is greater than that of the SUV_{max}, due to the utilization of multi-pixel ROIs [28]. Hence, SUV_{peak} values were also determined when analyzing the detected lesions, since it involves the mean of a few pixels at the hottest area of the lesion.

From our data, considering the physical decay of the radiotracer between PET/CT and PET/MRI scans (i.e., average of 87.51-min difference) and PET acquisition durations for comparable image qualities (24 vs. 6 min: 3 min/bed for eight beds in PET/CT and 1 min/bed for six beds in PET/MRI), the effective acquisition time difference between the two scans is approximately seven times (i.e., four times in acquisition time and 42 % reduction in count density from the physical decay).

In other words, comparable FDG PET data could be acquired using seven times lower injected dose with the TOF PET/MRI in this study if we acquire PET data in PET/MRI for the same duration as we acquired PET/CT data or seven times faster. This result is consistent with the theoretical estimation. In theory, using TOF in PET reconstruction, it is expected that the effective count is improved inversely proportional to the width of TOF timing (i.e., timing resolution) [3]. Hence, the SNR improvement in Poisson statistics as PET counting statistics generally follow, is inversely proportional to the square root of the timing resolution when the signal (i.e., counts) is linear and the noise is the square root of the number of counts. More specifically, the signal-to-noise improvement from TOF PET over non-TOF PET is proportional to $\sqrt{(2D/c\Delta t)}$ where D is the object diameter, c is the speed of light, and Δt is the timing resolution of TOF [29]. For example, from non-TOF to 400-ps TOF, based on this formula, the SNR improvement is approximately three times for an object size of 50 cm in diameter. In addition, there is a significant difference in the raw sensitivities of the PET detectors from our PET/CT scanners and PET/MRI used in this investigation. Furthermore, one of the advantages of TOF PET detector is its ability to have less noise even at a low count rate [17]. Decreasing the injected activity reduces noise equivalent count rate more slowly in TOF PET than in non-TOF PET, providing a further advantage with TOF PET. Based on the system specifications of the scanners, the improvement of the raw sensitivity is close to 3–5 times (from 8.4 cps/kBq for GE Discovery VCT PET/CT [30] and 4.9 cps/kBq for Siemens Biograph HiRez 16 [31] to 23.3 cps/kBq for GE Signa PET/MR). Combining these two factors, 5–7 times (approximately 3 times improvement of SNR from < 400-ps TOF performance multiplied by 2 times improvement of SNR from the raw sensitivity difference) of effective SNR improvement can be calculated, and our visual quality assessment is precisely in line with this theoretical
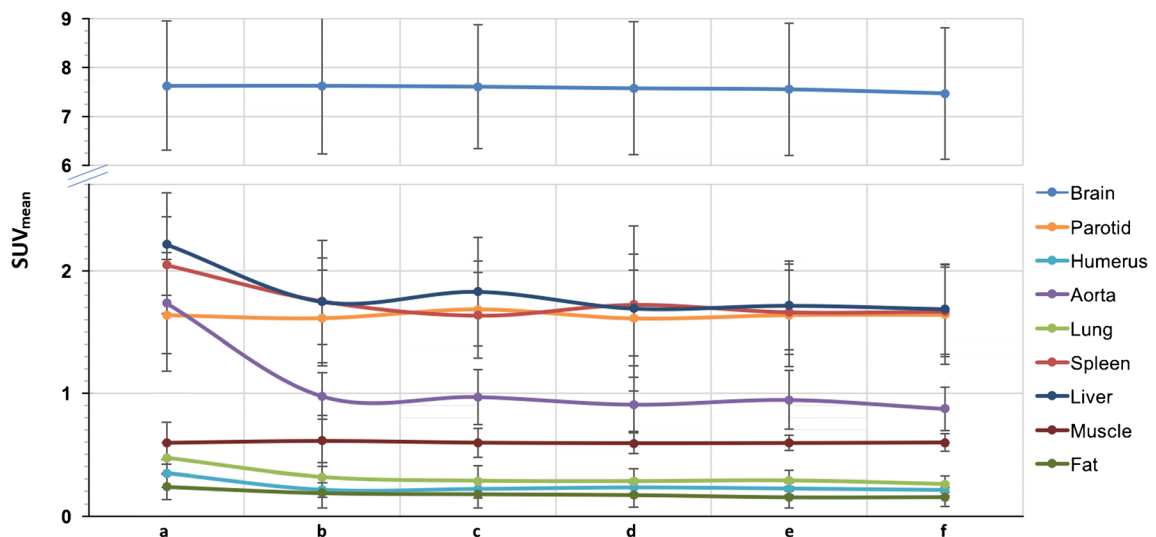
Fig. 3 Summaries of the SUV_{mean} for normal tissues determined via **a** PET/CT (non-TOF) images and PET/MR (TOF) images at **b** 0.25-min PET/MR, **c** 0.50-min PET/MR, **d** 1-min PET/MR, **e** 2-min PET/MR, and **f** 4-min PET/MR, along with the standard deviations.
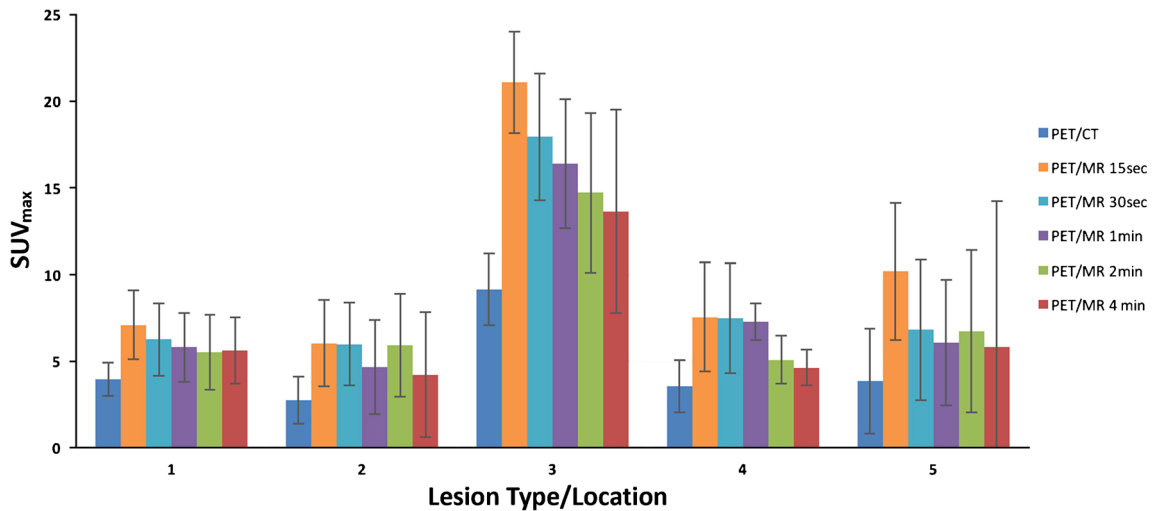
Fig. 4 Summaries of the SUV_{max} of PET/CT (non-TOF) images and PET/MR (TOF) images of detected lesions at 4, 2, 1, 0.50, and 0.25 min, along with the standard deviations. 1 Brown fat, 2 lymph node, 3 peritoneal implant, 4 pulmonary nodule, and 5 other. Lesions with sample sizes equal to or less than three, are grouped under "other".

estimation in improved sensitivity. By the way, we did not take into account the differences in system spatial resolutions between these scanners. In their respective system specifications, the spatial resolution measurements at 1 cm from the center of FOV are 6.3 and 6.1 mm, 5.12 and 5.18 mm, and 4.1 and 6.1 mm full-width at half maximum in transaxial and axial directions for Biograph HiRez 16, Discovery VCT, and SIGNA PET/MR, respectively. As these values show, the differences in spatial resolution measurements are difficult to objectively favor one system over another.

There are a few limitations to this study, the PET/MR and PET/CT acquisitions could not be done in a randomized order and not all acquisitions could be done 60 min post injection due to regulatory restrictions. In this study, we ensured the utilization of our institution's existing workflow. Another limitation is the patient population being low, this is due to the willingness of the subjects to participate. The relative number of lesions was also small and did not include bone or liver metastases. For the observed lesions, further analysis can be performed to differentiate between the contribution of TOF and additional uptake time to high SUV_{max}. However, even with a 1.5 h delayed PET/MR imaging (1.5 h later than PET/CT imaging), the results of this study show that this high-sensitivity SiPM-based TOF PET is able to provide better image quality as well as comparable standard uptake values. With TOF PET/MR, as
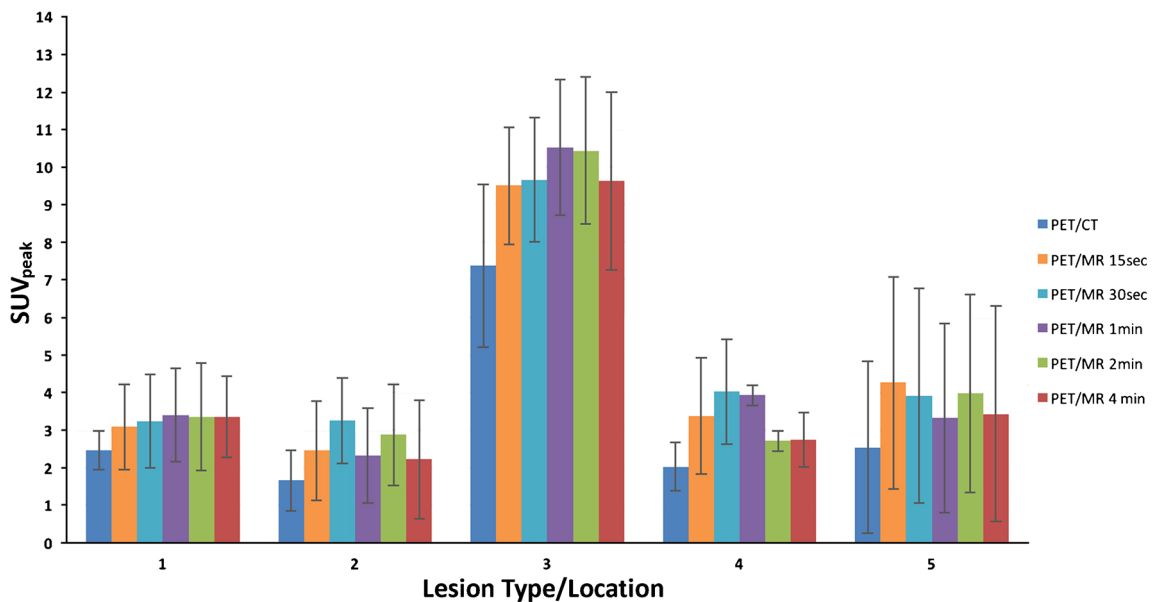

Fig. 5 Summaries of the SUV_{peak} of PET/CT (non-TOF) images and PET/MR (TOF) images of detected lesions at 4, 2, 1, 0.50, and 0.25 min, along with the standard deviations. 1 Brown fat, 2 lymph node, 3 peritoneal implant, 4 pulmonary nodule, and 5 other. Lesions with sample sizes equal to or less than three, are grouped under "other".

MRAC sequences only took less than 20 s, and were run simultaneously with PET, unlike with PET/CT, ensuring the scan time to be limited solely on PET acquisition.

As our data showed above, seven times reduction in either injection radiotracer dose for the same duration of scan or total whole-body scan time for the same amount of injected dose, this "ultra-sensitivity" PET detector provides a path to offer clinically acceptable extremely low-dose FDG PET studies. In addition, if we extend the total PET acquisition time a little further from the 4 min/bed we used in our PET/MRI investigation to, for example 6 min/bed, additional injected dose reduction is possible, still with the total study time well under 1 h for patient convenience. All of these data and analyses indicate that we can reduce the injected dose close to 10 times (7 times of reduction we already showed above, and additional scan time could further provide more reduction), resulting in less than 1 mCi of FDG for clinically comparable PET studies—10 times reduction from recommended 10–20 mCi injection according to the Procedure Guideline of Society of Nuclear Medicine and Molecular Imaging [18]. At this level of FDG injection, the effective dose is close to 1 mSv or potentially lower than 1 mSv (i.e., sub-mSv) in adults for tumor imaging. The extended PET acquisition time is particularly feasible with simultaneous PET/MR imaging when we take advantage of the long MR acquisitions. For this reason, for PET/MRI, seven times of scan time reduction (i.e., "ultrafast" PET) may not be desirable. The scan time advantage is more relevant if the similar raw sensitivity and TOF timing resolution are implemented in PET/CT since even diagnostic CT can be performed in a very short time.

Conclusion

Our study indicates that comparable visual quality and lesion SUV measurement are possible in much reduced PET acquisition time (or much reduced injected dose) when we utilized high-sensitivity (23.3 cps/kBq) 400 ps TOF PET in comparison to lower-sensitivity (8.4 and 4.9 cps/kBq) non-TOF PET. Approximately seven times dose reduction at a constant scan time or acquisition time reduction at an equal dose, did not result in poorer lesion detection or visual image quality degradation in our datasets, implying further dose/acquisition time reduction is possible with extended scan time for sub-mSv clinically acceptable FDG PET studies. Given the small sample size, further studies on how much dose/acquisition time reduction is possible are warranted.

References

1. Vandenberghe S, Mikhaylova E, D'Hoe E, Mollet P, Karp JS (2016) Recent developments in time-of-flight PET. EJNMMI Phys 3(1):3. https://doi.org/10.1186/s40658-016-0138-3
2. Karp JS, Surti S, Daube-Witherspoon ME, Muehllehner G (2008) Benefit of time-of-flight in PET: experimental and clinical results. J Nucl Med 49(3):462–470. https://doi.org/10.2967/jnumed.107.044834
3. Surti S, Kuhn A, Werner ME, Perkins AE, Kolthammer J, Karp JS (2007) Performance of Philips Gemini TF PET/CT scanner with special consideration for its time-of-flight imaging capabilities. J Nucl Med 48(3):471–480
4. Miller M, Zhang J, Binzel K et al (2015) Characterization of the Vereos digital photon counting PET system. J Nucl Med 56:434
5. Schmall JP, Wiener RI, Surti S, Ferri A, Gola A, Tarolli A, Piemonte C, Karp JS (2014) Timing and energy resolution of new near-UV SiPMs coupled to LaBr3:Ce for TOF-PET. IEEE Trans Nucl Sci 61(5):2426–2432. https://doi.org/10.1109/TNS.2014.2346579
6. David S, Jakob W, Peter Michael D et al (2015) PET performance and MRI compatibility evaluation of a digital, ToF-capable PET/MRI insert equipped with clinical scintillators. Phys Med Biol 60:7045
7. Martins P, Blanco A, Crespo P, Marques MFF, Marques RF, Gordo PM, Kajetanowicz M, Korcyl G, Lopes L, Michel J, Palka M, Traxler M, Fonte P (2014) Towards very high resolution RPC-PET for small animals. J Instrum 9(10):C10012. https://doi.org/10.1088/1748-0221/9/10/C10012
8. Beiderwellen KJ, Poeppel TD, Hartung-Knemeyer V, Buchbender C, Kuehl H, Bockisch A, Lauenstein TC (2013) Simultaneous 68Ga-DOTATOC PET/MRI in patients with gastroenteropancreatic neuroendocrine tumors: initial results. Investig Radiol 48(5):273–279. https://doi.org/10.1097/RLI.0b013e3182871a7f
9. Kadrmas DJ, Casey ME, Conti M, Jakoby BW, Lois C, Townsend DW (2009) Impact of time-of-flight on PET tumor detection. J Nucl Med 50(8):1315–1323. https://doi.org/10.2967/jnumed.109.063016
10. Taniguchi T, Akamatsu G, Kasahara Y, Mitsumoto K, Baba S, Tsutsui Y, Himuro K, Mikasa S, Kidera D, Sasaki M (2015) Improvement in PET/CT image quality in overweight patients with PSF and TOF. Ann Nucl Med 29(1):71–77. https://doi.org/10.1007/s12149-014-0912-z
11. Karlberg AM, Saether O, Eikenes L, Goa PE (2016) Quantitative comparison of PET performance-Siemens biograph mCT and mMR. EJNMMI Phys 3(1):5. https://doi.org/10.1186/s40658-016-0142-7
12. Lois C, Jakoby BW, Long MJ, Hubner KF, Barker DW, Casey ME, Conti M, Panin VY, Kadrmas DJ, Townsend DW (2010) An assessment of the impact of incorporating time-of-flight information into clinical PET/CT imaging. J Nucl Med 51(2):237–245. https://doi.org/10.2967/jnumed.109.068098
13. Zeimpekis KG, Barbosa F, Hüllner M, ter Voert E, Davison H, Veit-Haibach P, Delso G (2015) Clinical evaluation of PET image quality as a function of acquisition time in a new TOF-PET/MRI compared to TOF-PET/CT—initial results. Mol Imaging Biol 17(5):735–744. https://doi.org/10.1007/s11307-015-0845-5
14. Armstrong IS, James JM, Williams HA, Kelly MD, Matthews JC (2015) The assessment of time-of-flight on image quality and quantification with reduced administered activity and scan times in 18F-FDG PET. Nucl Med Commun 36(7):728–737. https://doi.org/10.1097/MNM.0000000000000305
15. Kadrmas DJ, Oktay MB, Casey ME, Hamill JJ (2012) Effect of scan time on oncologic lesion detection in whole-body PET. IEEE Trans Nucl Sci 59(5):1940–1947. https://doi.org/10.1109/TNS.2012.2197414
16. Hausmann D, Bittencourt LK, Attenberger UI, Sertdemir M, Weidner A, Büsing KA, Brade J, Wenz F, Schoenberg SO, Dinter DJ (2014) Diagnostic accuracy of 18F choline PET/CT using time-of-flight reconstruction algorithm in prostate cancer patients with biochemical recurrence. Clin Nucl Med 39(3):e197–e201. https://doi.org/10.1097/RLU.0b013e3182a23d37
17. Grant AM, Deller TW, Khalighi MM, Maramraju SH, Delso G, Levin CS (2016) NEMA NU 2-2012 performance studies for the SiPM-based ToF-PET component of the GE SIGNA PET/MR system. Med Phys 43(5):2334–2343. https://doi.org/10.1118/1.4945416
18. Delbeke D, Coleman RE, Guiberteau MJ, Brown ML, Royal HD, Siegel BA, Townsend DW, Berland LL, Parker JA, Hubner K, Stabin MG, Zubal G, Kachelriess M, Cronin V, Holbrook S (2006) Procedure guideline for tumor imaging with 18F-FDG PET/CT 1.0. J Nucl Med 47(5):885–895
19. Jones SC, Alavi A, Christman D, Montanez I, Wolf AP, Reivich M (1982) The radiation dosimetry of 2 [F-18]fluoro-2-deoxy-D-glucose in man. J Nucl Med 23(7):613–617
20. Kinahan PE, Fletcher JW (2010) PET/CT standardized uptake values (SUVs) in clinical practice and assessing response to therapy. Semin Ultrasound CT MR 31(6):496–505. https://doi.org/10.1053/j.sult.2010.10.001
21. Cheng G, Alavi A, Lim E, Werner TJ, Del Bello CV, Akers SR (2013) Dynamic changes of FDG uptake and clearance in normal

tissues. Mol Imaging Biol 15(3):345–352. https://doi.org/10.1007/s11307-012-0600-0

22. Cheng G, Torigian DA, Zhuang H, Alavi A (2013) When should we recommend use of dual time-point and delayed time-point imaging techniques in FDG PET? Eur J Nucl Med Mol Imaging 40(5):779–787. https://doi.org/10.1007/s00259-013-2343-9

23. Oldan JD, Turkington TG, Choudhury K, Chin BB (2015) Quantitative differences in [(18)F] NaF PET/CT: TOF versus non-TOF measurements. Am J Nucl Med Mol Imaging 5(5):504–514

24. Hamada K, Tomita Y, Ueda T, Enomoto K, Kakunaga S, Myoui A, Higuchi I, Yoshikawa H, Hatazawa J (2006) Evaluation of delayed 18F-FDG PET in differential diagnosis for malignant soft-tissue tumors. Ann Nucl Med 20(10):671–675

25. Iagaru A, Mittra E, Minamimoto R, Jamali M, Levin C, Quon A, Gold G, Herfkens R, Vasanawala S, Gambhir SS, Zaharchuk G (2015) Simultaneous whole-body time-of-flight 18F-FDG PET/MRI: a pilot study comparing SUVmax with PET/CT and assessment of MR image quality. Clin Nucl Med 40(1):1–8. https://doi.org/10.1097/RLU.0000000000000611

26. Koopman D, van Dalen JA, Lagerweij MC, Arkies H, de Boer J, Oostdijk AH, Slump CH, Jager PL (2015) Improving the detection of small lesions using a state-of-the-art time-of-flight PET/CT system

and small-voxel reconstructions. J Nucl Med Technol 43(1):21–27. https://doi.org/10.2967/jnmt.114.147215

27. Wahl RL, Jacene H, Kasamon Y, Lodge MA (2009) From RECIST to PERCIST: evolving considerations for PET response criteria in solid tumors. J Nucl Med 50(Suppl 1):122S–150S. https://doi.org/10.2967/jnumed.108.057307

28. Velasquez LM, Boellaard R, Kollia G, Hayes W, Hoekstra OS, Lammertsma AA, Galbraith SM (2009) Repeatability of 18F-FDG PET in a multicenter phase I study of patients with advanced gastrointestinal malignancies. J Nucl Med 50(10):1646–1654. https://doi.org/10.2967/jnumed.109.063347

29. Budinger TF (1983) Time-of-flight positron emission tomography: status relative to conventional PET. J Nucl Med 24(1):73–78

30. Teras M, Tolvanen T, Johansson JJ, Williams JJ, Knuuti J (2007) Performance of the new generation of whole-body PET/CT scanners: discovery STE and discovery VCT. Eur J Nucl Med Mol Imaging 34(10):1683–1692. https://doi.org/10.1007/s00259-007-0493-3

31. Brambilla M, Secco C, Dominietto M, Matheoud R, Sacchetti G, Inglese E (2005) Performance characteristics obtained for a new 3-dimensional lutetium oxyorthosilicate-based whole-body PET/CT scanner with the National Electrical Manufacturers Association NU 2-2001 standard. J Nucl Med 46(12):2083–2091